Supplementary Material on :
Implanted muon spin spectroscopy on 2-O-adamantane: A model system that mimics the liquid⟶glasslike transitions

M. Romanini, J.Ll Tamarit, L.C. Pardo
Grup de Caracterizacio de Materials, Departament de Fisica,
ETSEIB, Universitat Politecnica de Catalunya, Diagonal 647, 08028 Barcelona, Catalonia, Spain

F.J. Bermejo, R. Fernandez-Perea
Instituto de Estructura de la Materia,Consejo Superior de Investigaciones Cientificas,
Serrano 123, E-20886 Madrid, Spain

F.L. Pratt
ISIS Neutron and Muon Source, STFC Rutherford Appleton Laboratory,
Chilton, Didcot, Oxfordshire, OX11, 0QX, United Kingdom

December 2, 2016

The following sections provide a more in depth description of the calculations and measurements carried out in order to clarify the nature of the bound muon states as well as to provide additional checks on the physical soundness of phenomena explored using weak transverse fields.

S1 Magnetic properties of the muoniated radical

A summary of results obtained by running the DALTON code [1] is given in Table S1. A glance to data listed in the referred table shows that the precise values for the isotropic component A_{iso} are strongly dependent on the method of calculation employed, with Hartree-Fock estimates yielding values significantly above those predicted on the basis of Kohn-Sham DFT calculations performed using three different functionals. In contrast, the basis set dependence of the obtained results appears to be rather less marked. From the tabulated data and account made of previous experience using this kind of calculations [2, 3] we take the values obtained using correlation-consistent polarized valence double zeta basis (cc-pVDZ) and the B3PW91 functional as the more likely set. Such results for A_{iso} which come to be about twice the absolute value for acetone found by experiment and also its negative sign, suggest one possible reason for the lack of any clear resonance at the expected field values. Data pertaining the spin-dipolar contribution to the hyperfine coupling tensor, only available from DFT calculations also show a noticeable dependence with the employed basis set and thus serve to set some bounds to quantify this contribution if compared to A_{iso}. However, the absolute magnitude of the axial dipolar term D_1 is always roughly double A_{iso}.

The obtained data show a rather extreme sensitivity to the specific local molecular arrangement surrounding the Mu site. In particular, the results display a strong dependence on the value of the C-C-O-Mu dihedral angle θ_{Mu} so that the calculated values for A_{iso} appear to follow a $(1-\cos^2(\theta))$ law. The result is of some interest since motions involving such molecular internal coordinate are expected to appear at relatively low frequencies and therefore should be strongly coupled to intermolecular (phonon) degrees of freedom. In fact the quantum zero point vibrational motion of the Mu about the C=O axis has a very large effect on the hyperfine coupling, changing both the sign and magnitude of the A_{iso} coupling in this type of radical to leave a small positive value, as seen experimentally in acetone. When the dipolar ratio $|D_1/A_{iso}|$ is large, as it is here, the predicted resonance takes the form of a sharp rise or kink at field proportional to $|D_1/2 - A_{iso}|$ rather than following the conventional resonance line shape in the form of a dip that is seen for modest dipolar ratios. The case of the bond-centred muonium site

	Basis	A_{11}	A_{22}	A_{33}	A_{iso}	D_1	D_2
DFT/B3PW91	cc-pVDZ	-74.9	41.7	-99.0	-44.1	85.8	24.1
DFT/CAMB3LYP	cc-pVDZ	-70.7	47.5	-95.1	-39.4	86.9	24.4
DFT/B3LYP	cc-pVDZ	-69.8	47.6	-94.0	-38.7	86.3	24.2
DFT/B3LYP	6-311G**	-73.8	41.3	-93.3	-43.3	84.6	19.5
DFT/B3LYP	6-311G	-84.9	41.4	-100.4	-48.0	89.4	15.5
DFT/B3LYP	6-31G**	-72.3	41.0	-96.6	-42.6	83.6	24.3
HF	cc-pVDZ				-54.1		
HF	6-311G**				-54.5		
HF	6-311G				-62.5		
HF	6-31G**				-57.7		

Table S1: Calculated values for the hyperfine coupling constants (MHz) carried out at various levels of refinement. Computations have been carried out by means of the DALTON code [1] either at the Hartree-Fock level (HF) or Kohn-Sham density functional theory using the B3LYP, CAMB3LYP and B3PW91 functionals. The employed basis sets include correlation-consistent cc-pVDZ which are widely used for this kind of calculations. More extended basis sets were not used on account of the weak dependence of the results on the chosen basis (see text). The quantities A_{ij} stand for the principal values of the symmetrized (i.e. diagonal) HFC tensor at the muon site and D_1 and D_2 are the axial and non-axial dipolar anisotropy terms. All calculations have been carried out for optimized geometries where the C-C-O-Mu atoms lie within the same plane.

in Si provides perhaps the best known example of this behaviour [4]. There is evidence for this type of repolarisation behaviour in the present system in the form of a sharp jump in the LF data taking place around 2 kG within the SDP phase data measured at 150 K (see Fig.S2), which would correspond to a quantum corrected A_{iso} value of 16 MHz, taking D_1 to be 86 MHz. This A_{iso} value is comparable with the range of values seen in liquid acetone below room temperature [5].

S2 Field dependence of the muon relaxation rates and relaxation amplitudes

Several measurements were carried out in addition to those performed under a weak transverse field described in the main text. These pertain to experiments performed under zero (ZF) and longitudinal (LF) fields.

In general terms, measurements carried out under longitudinal fields provide decay rates, amplitudes and baseline values which are often significantly dependent upon temperature and applied field. This comes as a consequence of the fact that within such experimental configuration all paramagnetic and diamagnetic muons can contribute to the measured signal. The paramagnetic contribution from muonium is expected to follow exponential relaxation towards a baseline set by the diamagnetic fraction. As an attempt to disentangle the contribution of the different species to the observed relaxation, several measurements of the variation of the relaxation spectral parameters with applied field and temperature were carried out. The measurement aimed to test whether the majority of incoming muons ended up within molecular adducts, or whether a significant unreacted Mu fraction is present which could be revealed by its signature decoupling from the muonium electron, which is known to take place for fields above a characteristic value of 1600 G. Figure S1 displays the LF field dependence of the relaxation rates and Figure S2 displays the amplitudes for selected temperatures and fields up to 4000 G. Data shown in Figs. S1 and S2 display results for measurements carried out well within the rotator-phase crystal at a relatively high temperature (300 K) as well as within the monoclinic, positionally disordered phase well below the transition, namely at 150 K. Let us first discuss the data pertaining to the relaxation rate. Data concerning the measurement at 150 K display a visible maximum centered at about 20 G - 30 G which is superimposed on a far broader component. The latter, underlying component may be taken, as previously done in a study on two structural glasses [6, 7], as a map of the spectral density function for muonium diffusion as evidenced by the initial suppression for applied field values consistent with the muonium hyperfine field, namely $B_{hyp} 2\pi A_{Mu}/\gamma_e = 1600$ G corresponding to the established value of the hyperfine coupling constant $A_{Mu} = 4.5$ GHz , which is taken as an indication of rapid diffusive motions. However, as discussed in the previous section, the resonance/decoupling feature of the radical also occurs

in the 2 kG region, so there is considerable ambiguity in the interpretation of the relaxation behaviour in this case.

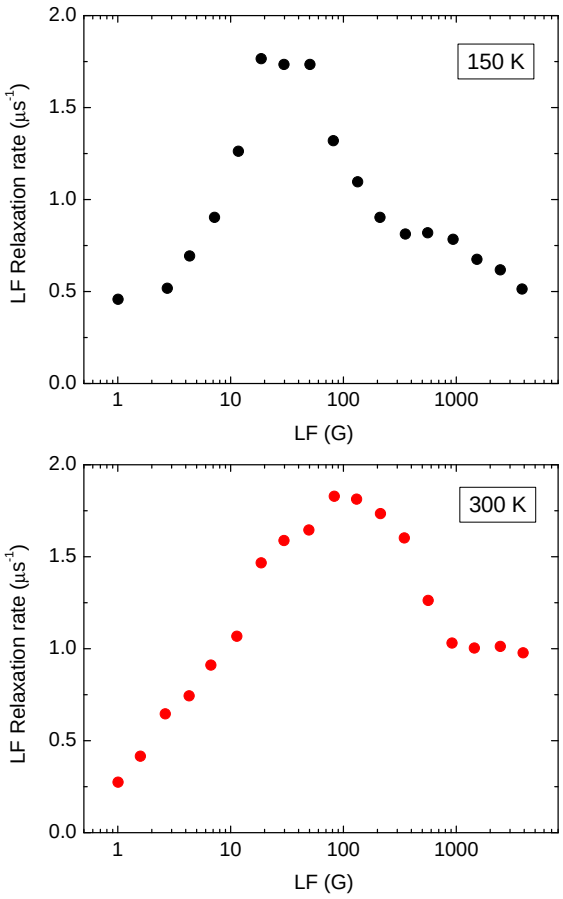

Figure S1: Longitudinal field dependence of the observed relaxation rates for characteristic temperatures below and above the phase transition

Data pertaining to the plastic crystalline phase are somewhat different since it shows a broad maximum at about 80 G that also sits on a broad background. The absence of any indication of suppression of the relaxation above 1000 G is interpreted as evidence of the far more complex muonium chemistry taking place within the rotationally disordered phase which may lead to the opening of channels for reaction pathways comparable to those in operation within the liquid state.

The data concerning the temperature dependence of the polarization which were measured for temperatures 150 K, 200 K, 250 K and 300 K, do show some features worth commenting on. In general terms as can be gauged from Fig.S2, the curves show a pretty large dependence with temperature, meaning that the effective hyperfine coupling tensor and the electronic relaxation rate are expected to be strongly dependent on temperature. As expected from what has been reported above concerning zero field studies, data concerning the plastic crystal starts at low fields from a far higher value than those pertaining to the monoclinic crystal due to dynamical reorientational averaging of the dipolar terms in the hyperfine tensor. Both curves display at low fields a gradual increase in polarization with increasing field resulting from decoupling of the muon spin from the local fields generated by nearby proton nuclear moments which usually amount to some tens of Gauss. Finally for fields larger than the muonium hyperfine field, namely 1600 G, one would expect a suppression of the relaxation which would be indicative of fast muonium diffusion.

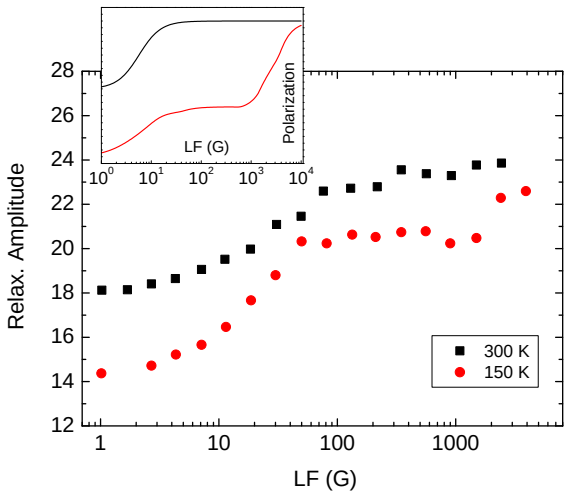

Figure S2: Longitudinal field dependence of the observed relaxation amplitudes for characteristic temperatures below and above the phase transition. The inset depicts the results of calculations of the field dependence of the polarization resulting from DFT/B3LYP calculations for a orientationally frozen radical with hyperfine constants A_{iso} = -40 MHz, D_1 = 56 MHz, D_2 = 14 MHz as shown by the red line as well as for the case of a fast rotating radical with corresponding values A_{iso} = -40 MHz, D_1 =D_2 = 0 MHz depicted by the black line. Both cases are taken as a rational to interpret the experimental data shown for the two quoted temperatures. The meaning of the various symbols is explained in Table S1.

S3 Zero field μSR

As mentioned in the main text, the presence of paramagnetic species will be felt by measurements under ZF conditions. Possible candidates having enough spin density to become detectable are Mu and the neutral adduct 2-O-adamantane-Mu. At zero field, the latter is expected to contribute to the relaxation with a fast relaxing component associated with the singlet-triplet transition in the corresponding Breit-Rabi diagram. Possible intratriplet transitions typically appearing at higher frequencies cannot reliably be observed at a pulsed source such as ISIS as they may lie outside the available frequency window. The relevant internal fields are here those hyperfine in origin characterized by a hyperfine coupling constant (hfcc) A_{iso} which for simplicity is assumed to be isotropic [8]. Such hfcc may exhibit some temperature dependence originated from vibrational or reorientational motions of some kind which involve changes in the orientation of the O-Mu bond. The real situation in the solid state is made much more complicated by the presence of hyperfine anisotropy and coupling to other spins in the system such as protons.

Similar difficulties as those mentioned above concerning the inclusion of dynamic effects here apply. In fact, for our case here, the most general form involves an integral equation such as [9],

$$P_z(t) = P_z(t)^{stat} \exp(-\nu_c t) + \nu_c \int_0^t P_z(t-t') P_z(t')^{stat} \exp(-\nu_c t') dt' \qquad (1)$$

where $\nu_c = 1/\tau_c$ is a correlation frequency and $P_z(t)^{stat}$ stands for a static field distribution which for the case in hand would correspond to the static Kubo-Toyabe form with a lorentzian distribution of local fields. The two limiting cases are easy to gauge from the formula given above. If the fluctuations are too slow, $\nu_c \longrightarrow 0$ one recovers the static case whereas in the opposite limit motional narrowing behaviour is recovered and relaxation conforms to single exponential behaviour. The criterium to judge which limit is closer to our experiment, if any, is given by the magnitude of the ratio $\nu_c/\gamma_\mu\Delta$. Plugging in data derived within the previous section concerning τ_c as well as Δ we found a range of values for such ratio within 1.2 - 12 which tells that at the higher temperatures we are well within motional narrowing and not too far away from it in most of the explored range. A sample of some of the measured spectra is shown in Fig S3. A glance to such plots reveals the non-exponential character of the observed relaxation which shows a fast decay well within the first microsecond followed by a far smoother decay at longer times.

The spectra plotted in Fig.S3 could be roughly approximated by a single exponential. A fast relaxing component needs to de added to account for data below 1 μs or so which become most noticeable at the

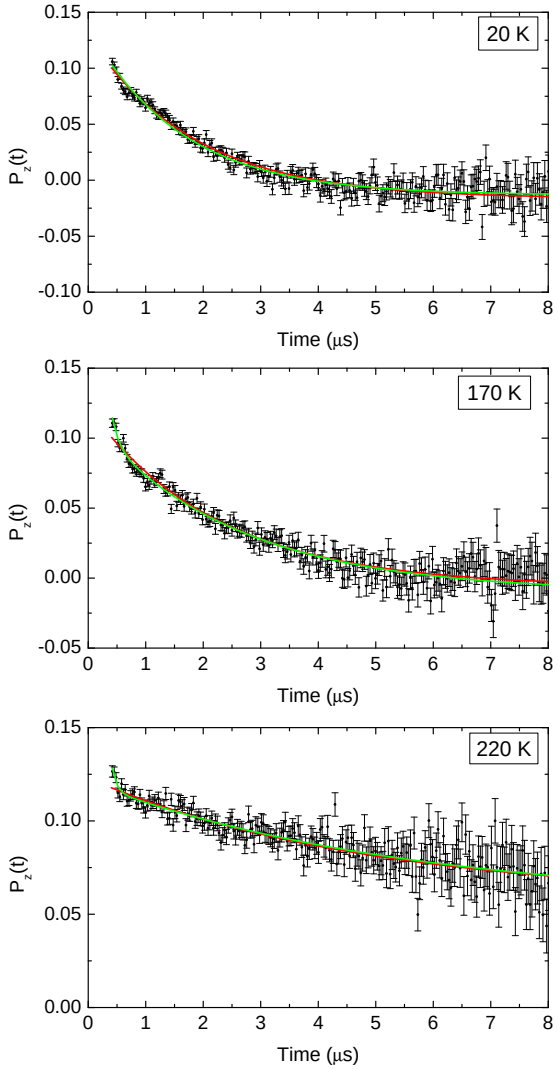

Figure S3: A sample of spectra measured under a zero applied field. The spectra correspond to the two extreme temperatures (20 K and 170 K) within which the relaxation rate follows the behaviour expected for a crystalline solid far away from critical regions as well as the temperature beyond which the relaxation rate only shows weak dependence with temperature. The solid red lines depict the best fits attained using a single-exponential relaxation function. Notice the departure from such a behaviour for times below one microsecond. Improved fits result if the two component fit of Eqn.2 is employed instead. The double exponential fits are shown by the solid green lines.

lowest temperatures. A sum of two exponential functions was able to account for all data although the ill-conditioned nature of the parameter estimation problem lead to statistically unreliable results. To ease the fitting effort, taking into account the validity of the approximation commented on above and also to avoid the numerical evaluation of Eqn.1 during the fitting process, the measurements were fitted using the following function with two well separated decay rates, which was found to describe the data well,

$$P_z(t) = \frac{a_0}{3}((2a_1(1-\lambda^s_{ZF}t)\exp(-\lambda^s_{ZF}t) + 2*(1-a_1)(1-\lambda^f_{ZF}t)\exp(-\lambda^f_{ZF}t) + 1) + bcgr \qquad (2)$$

where λ^f_{ZF} stands for a fast relaxing component, λ^s_{ZF} for the slow decay rate, a_0 is a global scaling constant , a_1 is a proportionality constant to account for the signal strength of the slow relaxing process which is allowed to be temperature dependent and *bcgr* is a small, background term which following

the same procedure as employed for the transverse field case was set to an average value calculated after a first fitting round . The equation given above basically comprises two lorentzian Kubo-Toyabe functions needed to account for the observed spectra. A formally more physically sound analysis could be pursued in terms of the dynamic Kubo-Toyabe function [10] which involves an integral equation which can be solved numerically for any given internal field distribution. The current data however is somewhat limited for the time range where double exponential behaviour can be seen by the naked eye, namely below about one microsecond, which made unpractical to follow such an approach.

The temperature dependence of the ZF parameters is then shown in Fig.S4.

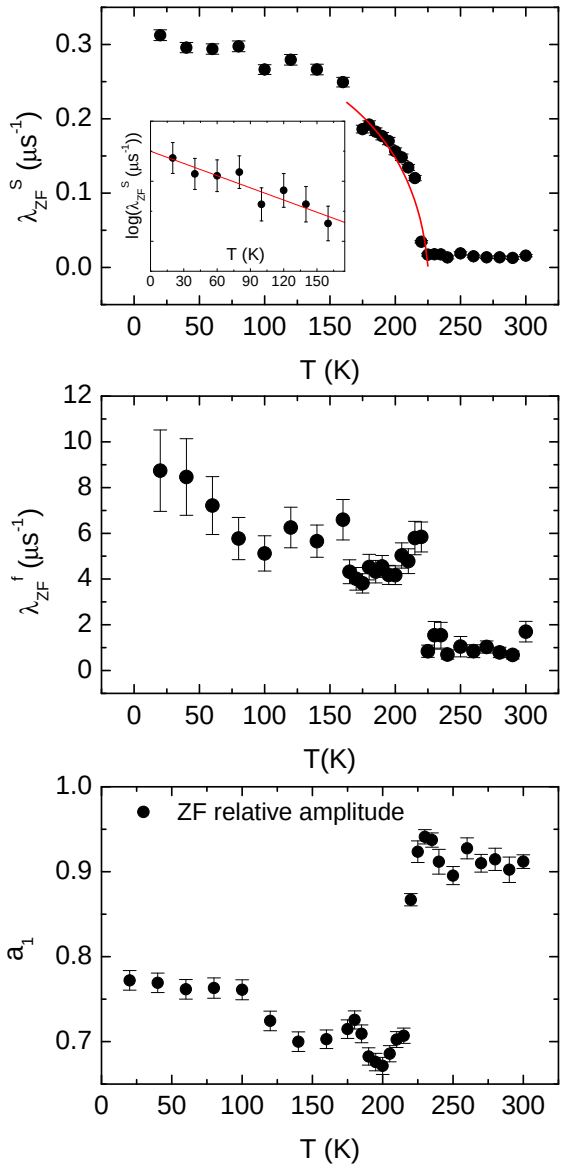

Figure S4: Temperature dependence of the observed relaxation rates for the slow (upper frame) and fast (lower frame) relaxation components. The solid lines depict fits to the low- and high temperature limits as described in the text. The line depicting the critical law following the square-root singularity has been calculated using a value of $T_c = 220.5$ K derived from fits to relaxation parameters pertaining μSR as described in the main text. Only a global scaling constant is used as a free parameter. The lower frame shows the temperature dependence of the a_1 constant employed to quantify the fraction of the slow relaxing species as shown in Eqn. 2

A comparison of the values of the relaxation rates with those derived for the transverse case shows that the values derived here are about double those obtained for the TF study.

The relaxation rate corresponding to the slower relaxing component λ_{ZF}^{s} mimics the behaviour of the data just discussed and can again be accounted for using Eqn.(5) of the main text. As a consistency check, the upper frame of Fig. S4 displays the calculated curve displaying the square-root law where the critical temperature was set to the value derived from the analysis of the TF data, so that only parameters concerning $\xi(T)$ of Eqn. (5) together with the A global scaling constant were left free to vary. The result shows that the ZF rates can be reasonably well accounted for using such an estimate for the critical temperature.

The temperature dependence of the rate for the fast process λ_{ZF}^{f} is also shown in Fig.S4. The relaxation rates for such process are now more than one order of magnitude larger than those derived for the slow relaxation and appear to show a less marked dependence with temperature. It becomes difficult to reach any definite conclusion regarding such process due to the large scatter in data points. Its origin could be plausibly be related to phenomena reported for solid C_{70} [11] which appear as a fast, unresolvable high-frequency component associated with the singlet$\longrightarrow$ triplet transition in their ZF measurements. Its relaxation rate was also found to decrease with temperature as a consequence of thermally activated motions which lead to an average out of the site non-equivalences of A_{iso}, which ultimately resulted in the appearance of well resolved lines at high enough temperatures where reorientational motion of the C_{70} was sufficiently fast.

As far as the temperature dependence of a_1, the shape of the curve depicted in the lower frame of Fig. S4 compares to that for a_{TF} shown in Fig. 3, apart from the region below 150 K which shows an increase as the temperature is decreased. Such a feature has also been found in our previous studies on structural glasses (see the lower frame of Fig.1 in Ref. [7]) and was there interpreted as a signature of the temperature dependence of the muonium fraction. Similar features have been reported from studies of muon spin relaxation in H_2O ice [12] where also paramagnetic and diamagnetic species were detected in LF relaxation studies and there were found to be two well separated scales for the relaxation rate of the diamagnetic $\lambda_d \leq 0.05\mu s^{-1}$ and paramagnetic $\lambda_p \geq 10\mu s^{-1}$ components.

References

[1] K. Aidas *et al.* WIREs Comput. Mol. Sci. **4** 269, (2014) (doi: 10.1002/wcms.1172); Dalton, a molecular electronic structure program, Release Dalton2016 (2015), see http://daltonprogram.org.

[2] P. Verma, A. Perera, J.A. Morales, J.Chem.Phys. **139** 174103 (2013).

[3] B. Fernandez, P. Joergensen, J. Simons, J. Chem.Phys. **98**, 3060 (1993).

[4] F.L. Pratt, Phil. Mag. Lett. **75**, 371 (1997).

[5] D. Buttar, R.M. Macrae, B.C. Webster and E. Roduner, Hyp. Int. **65**, 927 (1990).

[6] F. J. Bermejo, I. Bustinduy, M. A. Gonzalez, S. H. Chong, C. Cabrillo, S. F. J. Cox, Phys. Rev. **B 70**, 214202 (2004).

[7] C. Cabrillo, F. J. Bermejo, S. F. J. Cox, Phys. Rev. **B 67**, 184201 (2003).

[8] In general, for crystalline environments one expects the hyperfine couplings to be fully anisotropic and thus dependent on the angles of such a tensorial quantity and the nearby proton spins. At any rate, in circumstances where dipolar couplings are expected to average out due to fast reorientational motion such occurs within the RP phase, only flip-flop transitions involving muon and proton spins driven by A_{iso} are relevant.

[9] A. Dalmas de Reotier Yaouanc, *Muon Spin Rotation, Relaxation and Resonance*, Oxford University Press, 2011, Oxford U.K., chapt. 6, p. 119.

[10] R. S. Hayano, Y. J. Uemura, J. Imazato, N. Nishida, T. Yamazaki, and R. Kubo, Phys.Rev. **B 20**, 850 (1979).

[11] R. M. McRae *et al.*, J. Phys.Chem **98**, 12133 (1994).

[12] S.F.J. Cox *et al.* Hyperf.Inter. **85**, 67 (1994); S.F.J. Cox, Phys.Scr. T **45**, 292 (1992); S.F.J. Cox, J.A.S. Smith, M.C.R. Symons, Hyperf.Inter. **65**, 993 (1990).